Electronic Supplementary Material (ESI) for RSC Advances.

Self-assembly of L-Phenylalanine Amino Acid: Electrostatic Induced Hindrance of Fibril Formation

Deepak Tomar[†], Shilpi Chaudhary[†] and Kailash Chandra Jena[†,‡,*]

[†]Department of Physics, Indian Institute of Technology Ropar, Rupnagar, Punjab-140001, India.

[‡]Center for Biomedical Engineering, Indian Institute of Technology Ropar, Rupnagar, Punjab-140001, India

AUTHOR INFORMATION

Corresponding Author

[*]Email : kcjena@iitrpr.ac.in.

Listing of contents

References

Supporting Information

1. Attenuated Total Reflection (ATR) Correction Method

The absorbance of IR radiation by the molecules present in the sample solution can be defined by Beer-Lambert law, given as:

$$Absorbance = \log\left(\frac{1}{T}\right) = \log\left(\frac{I_0}{I}\right) = \varepsilon c L \tag{1}$$

where, T is transmittance, I_o and I are the transmitted intensity of the empty cell (ATR background) and cell filled with sample (sample spectra), respectively, ε is the molar extinction coefficient or molar absorptivity, c is molar concentration and L is sample path length.

In ATR-FTIR process, the IR beam is allowed to incident on face of the crystal surface at an angle grater then critical angle (in our case the incident angle is 45°) reflects at the interface between crystal and sample. The transmitted IR beam penetrates into the sample and generate an evanescent wave perpendicular to the total internal surface of the crystal.[1] The electric field component of the evanescent wave follows an exponential decay profile at the interface and defined as:[2]

$$\mathrm{E} = \mathrm{E}_0 \exp\left(-\mathrm{z}/\mathrm{d}_\mathrm{p}\right) \tag{2}$$

where, E is the amplitude of electric field at a penetration distance of z, E_o is amplitude of electric field at interface between crystal and sample, and d_p is the distance, where the amplitude of the electromagnetic radiation falls (1/e) of the original value, called penetration depth defined as:[2-5]

$$d_p = \frac{\lambda}{2\pi\, n_1 \sqrt{\left(\sin^2\theta - (n_2/n_1)^2\right)}} \tag{3}$$

where, λ is the wavelength of incident radiation beam, θ is effective angle of incidence, n_1 and n_2 are the refractive indices of the ATR crystal) and the sample, respectively.

Since the incident IR radiation has electromagnetic field *E* that induces polarization *P*. Then the relation between incident electromagnetic field *E* and induced polarization *P* is considered upon linear and nonlinear optical interactions of light in bulk as well as surface, and given as:[6]

$$\mathrm{P} = \varepsilon_0 \chi^{(1)} \mathrm{E} + \frac{1}{2}\varepsilon_0 \chi^{(2)} \mathrm{EE} + \frac{1}{6}\varepsilon_0 \chi^{(3)} \mathrm{EEE} + \ldots \tag{4}$$

where ε_0 represents vacuum permittivity and $\chi^{(1)}, \chi^{(2)}, \chi^{(3)}, \ldots$ are first, second, third order electric susceptibilities and so on. In the present study we are keen to observe the IR absorption events dominated by linear optical interactions. For which the ATR-FTIR spectroscopic tool is used for performing experiments. So in the present study, the contributions from higher order susceptibility terms are negligible. The absorption of molecules is specified by imaginary part of the linear susceptibility. In addition the imaginary spectra directly related to the concentration of sample molecules in the solution. So we are interested to obtain $\mathrm{Im}[\chi^{(1)}]$ line shapes instead of $|\chi^{(1)}|$. For retrieving $\mathrm{Im}[\chi^{(1)}]$ data, raw absorption data treated with ATR correction. The ATR correction factor (c_{ATR}) is given as:[2-6]

$$c_{\mathrm{ATR}} \propto \frac{2 n_1 \cos\theta}{N_R d_p \omega_{\mathrm{IR}}} \tag{5}$$

where, ω_{IR} is frequency of IR radiation beam, N_R is total number of reflections in contact with sample and imaginary part of linear susceptibility defined as:

$$\mathrm{Im}[\chi^{(1)}] = c_{ATR} A_{ATR} \tag{6}$$

where, A_{ATR} is the raw absorption data obtained from ATR-FTIR experiment. In our current study the ATR correction were performed by taking the dispersion data for ZnSe crystal from Connolly *et al.*[7], for diamond crystal from Phillip *et al.*[8] , and for water from Segelstein[9]. Our experimental results from the above method were in good agreement with the recently published data by Roy et al. for the evanescent wave penetration depth.[6]

2. Supporting figures

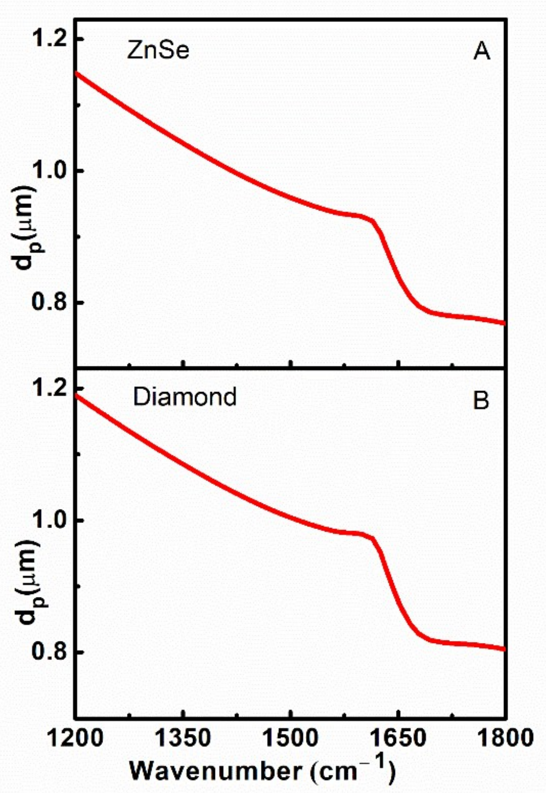

Figure S1. Penetration depth profile evanescent wave in pristine water at (A) ZnSe ATR crystal, and (B) diamond ATR crystal as a function IR radiation at an effective angle of incidence 45°.

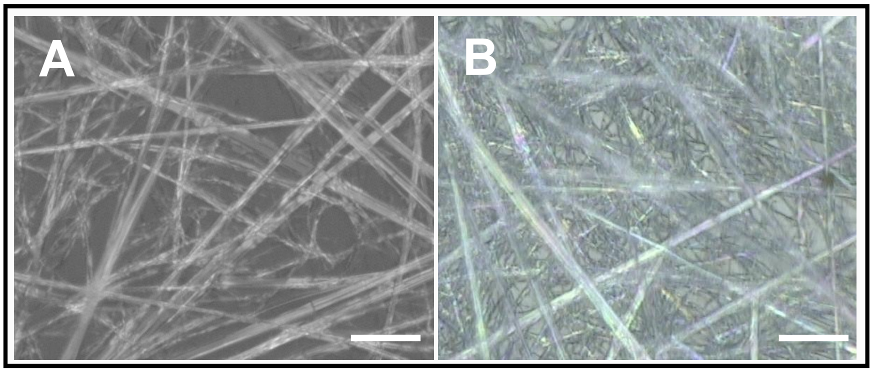

Figure S2. Optical microscopic images of the dried L-Phe samples prepared from the pH 5.8 aqueous solutions at 50 mM concentration. Samples were dried at room temperature (panel a) and at 50 °C in the oven (panel b), represented by 50μm white scale bars, respectively.

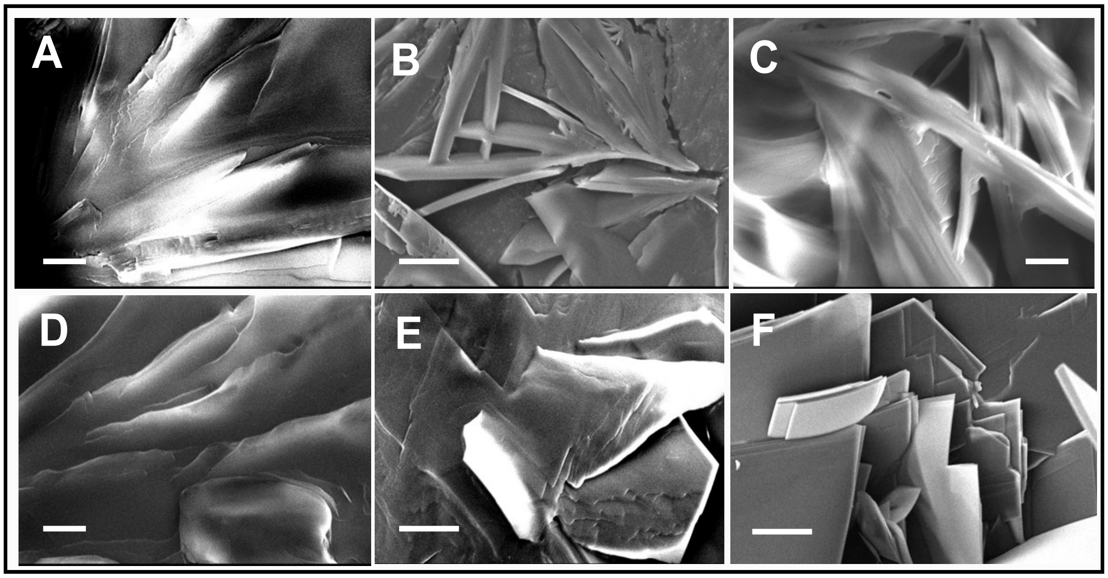

Figure S3. Morphology by SEM images of DL-Phe amino acid at various concentrations. Images represent the morphology of DL-Phe dried samples at pH 5.8 for (A) 0.01 mM, (B) 0.5 mM, (C) 1 mM, (D) 5 mM, (E) 50 mM, and (F) 150 mM. Scale bars shown in white for (A), (C), and (D) SEM images are 2μm; 10μm for (B), (E) and (F), respectively.

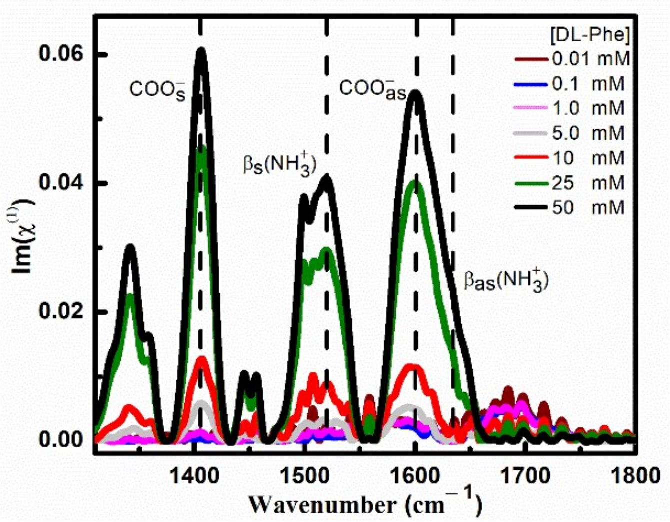

Figure S4. ATR-FTIR absorption spectra at ZnSe-water interface for various DL-Phe concentrations from 0.01 to 50 mM at pH 5.8. Dashed lines represent the various characteristic vibrational frequencies of amine and carboxylate groups.

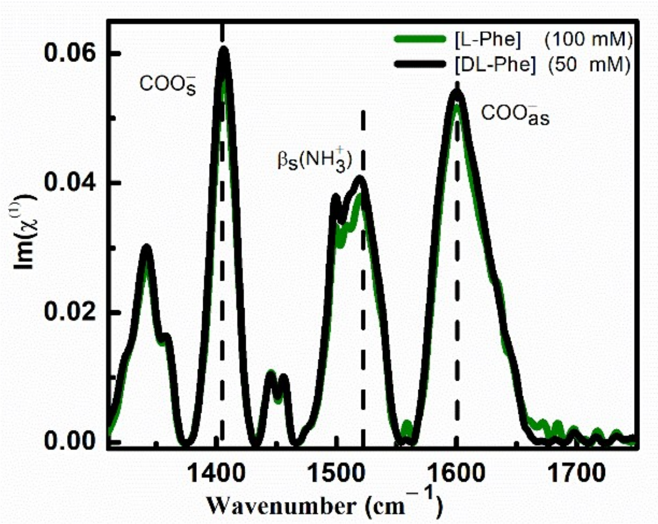

Figure S5. Comparison of ATR-FTIR vibrational spectral signatures of L- and DL-Phe in aqueous solution at 100 mM and 50 mM, respectively.

Table S1. Energy difference between the individual peak positions of respective aromatic protons for the three different pH environments.

pH variation	H_a (Ha$_1$ – Ha$_2$)[a] peak position (ppm)	difference (ppm)
1.5	7.345 - 7.328	0.017
5.8	7.339 - 7.320	0.019
12.2	7.293 - 7.275	0.018
pH variation	H_a (Ha$_2$ – Ha$_3$)[a] peak position (ppm)	difference (ppm)
1.5	7.328 - 7.309	0.019
5.8	7.320 - 7.304	0.016
12.2	7.275 - 7.256	0.019
pH variation	H_b (H_{b1} – H_{b2})[b] peak position (ppm)	difference (ppm)
1.5	7.297 - 7.280	0.017
5.8	7.284 - 7.266	0.018
12.2	7.218 - 7.200	0.018
pH variation	H_c (H_{c1} – H_{c2})[c] peak position (ppm)	difference (ppm)
1.5	7.232 - 7.217	0.015
5.8	7.225 - 7.208	0.017
12.2	7.182 - 7.165	0.017
pH variation	H_a (Ha$_3$) – H_b (H_{b1}) peak position (ppm)	difference (ppm)
1.5	7.309 - 7.297	**0.012**
5.8	7.304 - 7.284	**0.020**
12.2	7.256 - 7.218	**0.038**
pH variation	H_b (H_{b1}) – Hc (H_{c1}) peak position (ppm)	difference (ppm)
1.5	7.297 - 7.232	**0.065**
5.8	7.284 - 7.225	**0.059**
12.2	7.218 - 7.182	**0.036**

[a] Ha$_1$, Ha$_2$, and Ha$_3$ are the peak positions correspond to aromatic proton H_a.

[b] H_{b1} and H_{b2} are the peak positions correspond to aromatic proton H_b.

[c] $H_{c1}$and H_{c2} are the peak positions correspond to aromatic proton H_c.

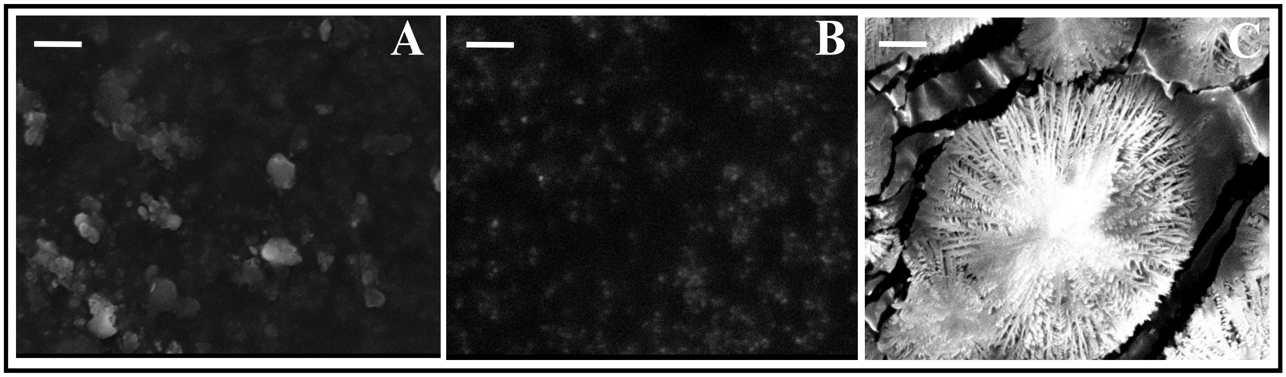

Figure S6. Structural morphology of the dried aqueous samples at three different pH values without the presence of L-Phe. SEM images of the dried samples at (A) pH 1.5; (B) pH 5.8; and (C) pH 12.2, represented with 2μm scale bars.

References

(1) J. M. Andanson and A. Baiker, *Chem. Soc. Rev.,* 2010, **39**, 4571-4584.

(2) M. R. Pereira and J. Yarwood, *J. Polym. Sci. Part B: Polym. Phys.,* 1994*,* **32**, 1881-1887.

(3) N. Harrick, *J. Opt. Soc. Am.,* 1965*,* **55**, 851-856.

(4) N. Harrick and F. Du Pre, *Appl. Opt.,* 1966*,* **5**, 1739-1743.

(5) L. A. Averett, P. R. Griffiths and K. Nishikida, *Anal. Chem.,* 2008*,* **80**, 3045-3049.

(6) S. Roy, P. A. Covert, T. A. Jarisz, C. Chan and D. K. Hore, *Anal. Chem.,* 2016*,* **88**, 4682-4691.

(7) J. Connolly, B. diBenedetto and R. Donadio, *Tech. Symp. East,* 1979*,* 141-144.

(8) H. Phillip and E. Taft, *Phys. Rev.,* 1964*,* **136**, A1445-A1448.

(9) D. J. Segelstein, *The Complex Refractive Index of Water*, M.Sc. Thesis, University of Missouri, Kansas City, 1981.